The Role of Stochastic and Modal Gating of Cardiac L-Type Ca^{2+} Channels on Early After-Depolarizations

Antti J. Tanskanen,*† Joseph L. Greenstein,*† Brian O'Rourke,‡¶ and Raimond L. Winslow*†¶
*Center for Cardiovascular Bioinformatics and Modeling, †The Whitaker Biomedical Engineering Institute, ‡Department of Medicine Division of Cardiology, and ¶The Institute for Molecular Cardiobiology, The Johns Hopkins University School of Medicine and Whiting School of Engineering, Baltimore, Maryland

ABSTRACT Certain signaling events that promote L-type Ca^{2+} channel (LCC) phosphorylation, such as β-adrenergic stimulation or an increased expression of Ca^{2+}/calmodulin-dependent protein kinase II, promote mode 2 gating of LCCs. Experimental data suggest the hypothesis that these events increase the likelihood of early after-depolarizations (EADs). We test this hypothesis using an ionic model of the canine ventricular myocyte incorporating stochastic gating of LCCs and ryanodine-sensitive calcium release channels. The model is extended to describe myocyte responses to the β-adrenergic agonist isoproterenol. Results demonstrate that in the presence of isoproterenol the random opening of a small number of LCCs gating in mode 2 during the plateau phase of the action potential (AP) can trigger EADs. EADs occur randomly, where the likelihood of these events increases as a function of the fraction of LCCs gating in mode 2. Fluctuations of the L-type Ca^{2+} current during the AP plateau lead to variability in AP duration. Consequently, prolonged APs are occasionally observed and exhibit an increased likelihood of EAD formation. These results suggest a novel stochastic mechanism, whereby phosphorylation-induced changes in LCC gating properties contribute to EAD generation.

INTRODUCTION

Single cardiac L-Type Ca^{2+} channels (LCCs) exhibit four distinct gating modes (Hess et al., 1984; Tsien et al., 1986; Yue et al., 1990). Mode 0 is a silent mode. Mode 0_a is a low-activity mode characterized by sparse, brief openings. Modes 1 and 2 are high-activity modes displaying bursts of brief or long-lasting openings, respectively. Although first identified in experiments using barium (Ba^{2+}) as the charge carrier (Hess et al., 1984; Yue et al., 1990), mode 2 gating of LCCs has been demonstrated recently to occur at physiological concentrations of extracellular calcium (Ca^{2+}) (Josephson et al., 2002a).

Several phosphorylation-related events regulate the fraction of LCCs gating in each mode. β-adrenergic receptor (β-AR) agonists induce protein kinase A (PKA)-mediated phosphorylation of the LCC α_{1C} subunit at the Ser1928 residue (Gao et al., 1997; De Jongh et al., 1996; Yoshida et al., 1992). This phosphorylation increases both the fraction of LCCs available for gating as well as the fraction gating in mode 2 (Chen-Izu et al., 2000; Yue et al., 1990). The signaling molecule Ca^{2+}/calmodulin-dependent protein kinase II (CaMKII), through phosphorylation of an as yet unidentified cell membrane protein(s), increases the fraction of LCCs gating in mode 2 relative to other modes (Dzhura et al., 2000). LCC agonists such as BayK8644 also increase mode 2 activity (Hess et al., 1984), potentially by inhibiting channel dephosphorylation or through allosteric interactions that mimic the effects of phosphorylation (Erxleben et al., 2003).

Early after-depolarizations (EADs) are depolarizations of membrane potential occurring during phases 2 or 3 of the cardiac action potential (AP). They are thought to be a possible trigger for development of polymorphic ventricular tachycardia (Roden, 1993; Zhou et al., 1992). Occurrence of EADs is often associated with prolongation of AP duration (APD, at 90% repolarization) produced, for example, by the action of LCC agonists (January and Riddle, 1989; January et al., 1988; Marbán et al., 1986) or by block of repolarizing potassium currents (Marbán et al., 1986). Cardiac myocytes can also exhibit EADs in response to β-adrenergic agonists such as isoproterenol (ISO) (De Ferrari et al., 1995; Volders et al., 1997), even at ISO concentrations producing shortening of APD (Priori and Corr, 1990). Recently, Wu et al. (2002) investigated AP properties in cardiac ventricular myocytes isolated from transgenic mice expressing a constitutively active form of CaMKII, which would be expected to induce an increase in the number of LCCs gating in mode 2 (Dzhura et al., 2000). These mice exhibited APD prolongation accompanied by frequent EADs. A CaMKII inhibitory peptide AC3-I eliminated EADs with little APD shortening (Wu et al., 2002). In addition, blockers of PKA and CaMKII have been shown to eliminate EADs and torsade de pointes in ventricular myocytes isolated from rabbits (Mazur et al., 1999).

These data suggest the hypothesis that factors which promote mode 2 gating of LCCs may be linked with the generation of EADs. We test this hypothesis using an ionic model of the canine ventricular myocyte incorporating stochastic gating of LCCs and ryanodine-sensitive Ca^{2+} release channels (RyRs) (Greenstein and Winslow, 2002).

Submitted August 17, 2004, and accepted for publication October 5, 2004.

Address reprint requests to Antti Tanskanen, The Johns Hopkins University, Clark Hall, Rm. 204, 3400 N. Charles St., Baltimore, MD 21218. E-mail: atanskan@bme.jhu.edu.

© 2005 by the Biophysical Society

0006-3495/05/01/85/11 $2.00

doi: 10.1529/biophysj.104.051508

The model is extended to describe mode 2 gating of LCCs, and is then used to simulate myocyte responses to 1 μM ISO.

Results demonstrate that random fluctuations in the number of open LCCs during the plateau phase of the AP can generate EADs. The most important fluctuations are those of LCCs gating in mode 2 and exhibiting long open times, which drive the slow-timescale fluctuations of L-type Ca^{2+} current (I_{CaL}). EADs occur randomly, and the likelihood of occurrence is an increasing function of the fraction of LCCs gating in mode 2. These results suggest a novel mechanism whereby phosphorylation-induced changes in LCC gating properties contribute to EAD generation.

METHODS

Simulations are performed using a recently developed canine ventricular myocyte model which incorporates stochastic gating of LCCs and RyRs within a large number of Ca^{2+} release units (Greenstein and Winslow, 2002). This model is able to reproduce experimentally measured properties of Ca^{2+}-induced Ca^{2+} release such as graded release, voltage dependence of excitation-contraction coupling gain, stable release termination, and the relative magnitude of voltage- versus Ca^{2+}-dependent inactivation of LCCs. The model has been extended to describe the action of 1 μM ISO on both Ca^{2+} regulatory proteins and ion channels of the cardiac ventricular myocyte (Greenstein et al., 2004). Details of model development, as well as a comparison of model Ca^{2+} transients and APs with and without ISO to those measured experimentally are provided in the following.

The local-control myocyte model

Simulations are performed using a canine ventricular myocyte model incorporating stochastic gating of LCCs and RyRs (Greenstein and Winslow, 2002). The model incorporates 1), sarcolemmal ion currents of the Winslow et al. (1999) canine ventricular cell model; 2), continuous-time Markov chain models of the rapidly activating delayed rectifier potassium (K^+) current I_{Kr} (Mazhari et al., 2001), the Ca^{2+}-independent transient outward K^+ current I_{to1} (Greenstein et al., 2000), and the Ca^{2+}-dependent transient outward chloride (Cl^-) current I_{to2}; 3), a continuous-time Markov chain model of I_{CaL} in which Ca^{2+}-mediated inactivation occurs via the mechanism of mode-switching (Imredy and Yue, 1994; Jafri et al., 1998); 4), an RyR channel model adapted from that of Keizer and Smith (Jafri et al., 1998; Keizer et al., 1998); and 5), locally controlled Ca^{2+}-induced Ca^{2+} release from junctional sarcoplasmic reticulum (JSR) via inclusion of LCCs, RyRs, Cl^- channels, and local JSR and diadic subspace compartments within Ca^{2+} release units (CaRUs).

The L-type Ca^{2+} channel gating scheme

The gating scheme of the LCC model is shown in Fig. 1 and has been described previously (Greenstein and Winslow, 2002; Jafri et al., 1998; Rice et al., 1999). Briefly, upper-row states encompass Mode Normal and lower-row states encompass Mode Ca. Each mode contains an open state (denoted O and O_{Ca}). Depolarization promotes transitions from left to right toward the open states. Elevation of subspace Ca^{2+} promotes transitions from Mode Normal to Mode Ca. When LCCs gate in Mode Ca, transitions into state O_{Ca} are infrequent. Mode Ca therefore corresponds to Ca^{2+}-inactivated states. Transition rates from Mode Ca to Mode Normal (i.e., recovery from Ca^{2+}-mediated inactivation) are Ca^{2+}-independent. The LCC also contains a separate voltage-dependent inactivation gate (not shown in Fig. 1) whose open probability decreases with membrane depolarization.

In this cell model, I_{CaL} is a function of the total number of channels (N_{LCC}), single-channel current magnitude (i), open probability (p_o), and the fraction of channels that are available for activation (f_{active}), where $I_{CaL} = N_{LCC} \times f_{active} \times i \times p_o$ (Handrock et al., 1998). The product $N_{LCC} \times f_{active}$ is chosen such that the amplitude of the whole-cell current agrees with that measured experimentally in canine myocytes (Hobai and O'Rourke, 2001). This approach yields a value of 50,000 for $N_{LCC} \times f_{active}$, consistent with experimental estimates of active LCC density (McDonald et al., 1986; Rose et al., 1992) and corresponding to 12,500 active CaRUs.

The number of CaRUs simulated explicitly need not be equal to the actual number of CaRUs in a cell. In simulations including a reduced number of CaRUs, total fluxes between the cytosol and the population of simulated CaRUs are scaled by the ratio $N_{actual}/N_{simulated}$ to maintain an average flux independent of the number of CaRUs simulated. No variance-reduction methods were used, hence use of reduced numbers of CaRUs increases the standard deviation of the scaled currents/fluxes by a factor of $\sim(N_{actual}/N_{simulated})^{1/2}$. Unless stated otherwise, all simulations in this study are performed using a minimum of 10,000 simulated CaRUs, which results in no greater than an ~2.2-fold increase in standard deviation of I_{CaL} compared to the full 50,000-CaRU model. This approach was a necessary compromise between model accuracy and tractability.

Stochastic simulation

The algorithm for solving the stochastic ordinary differential equations defining the model has been described previously (Greenstein and Winslow, 2002). Briefly, transition rates for each channel are determined by their gating schemes and their dependence on local Ca^{2+} level. Stochastic simulation of CaRU dynamics is used to determine all Ca^{2+} flux into and out of each local subspace. The summation of all Ca^{2+} fluxes crossing the CaRU boundaries is taken as inputs to the global model, which is defined by a system of coupled ordinary differential equations. The dynamical equations defining the global model are solved using the Prince-Dormand algorithm (Engeln-Müllges and Uhlig, 1996) which has been modified to embed the stochastic CaRU simulations within each time step. The Mersenne Twister (Matsumoto and Nishimura, 1998) random number generator algorithm (period = $2^{19,937} - 1$) is used in stochastic computations.

This model provides the ability to investigate the ways in which LCC, RyR, and subspace properties impact on Ca^{2+}-induced Ca^{2+} release and the integrative behavior of the myocyte. However, this ability is achieved at a high computational cost: up to 1 s of model activity was simulated in 3 min of simulation time with 1,250 CaRUs, and in 22 min with 12,500 CaRUs when running on 20 IBM Power4 processors configured with 4 gigabytes memory each.

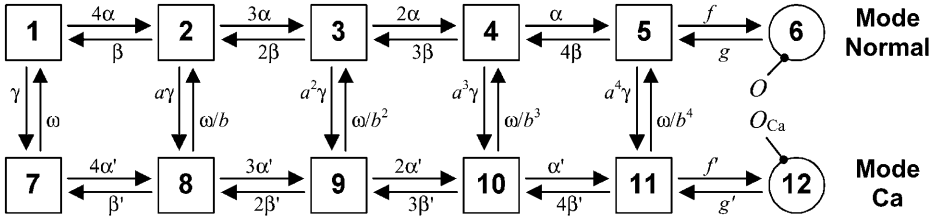

FIGURE 1 Markov model describing L-type Ca^{2+} channel. Top row describes Mode Normal; lower row, Mode Ca. States O and O_{Ca} are open states; all other states are closed.

Model of β-AR responses

β-AR agonists increase LCC availability (f_{active}; Chen-Izu et al., 2000; Herzig et al., 1993; Yue et al., 1990). In guinea pig and human ventricular myocytes, baseline values of f_{active} are relatively low and are increased by 2- to 2.5-fold in response to β-AR stimulation (or in heart failure, in which there may be hyperphosphorylation of LCCs; Chen et al., 2002; Handrock et al., 1998; Herzig et al., 1993; Schröder et al., 1998; Yue et al., 1990). These data differ from those in rat, which show considerably higher baseline availability and a smaller change in f_{active} in response to β-AR stimulation (Chen-Izu et al., 2000). We have therefore elected to develop a ''baseline'' model of β-AR action using data primarily from guinea pig, canine, and human ventricular myocytes (Greenstein et al., 2004). β-AR-induced phosphorylation of LCCs is modeled by including populations of both active (phosphorylated) and inactive (unphosphorylated) LCCs. Model parameters are adjusted based on analyses of slow cycling between active and inactive modes in the presence of ISO, indicating that at 1 μM concentration, ~25% of LCCs are available under control conditions, and that this increases to ~60% in the presence of ISO (Herzig et al., 1993), which corresponds to 30,000 active CaRUs out of a total of 50,000 simulated CaRUs. The fraction of active CaRUs is set equal to the fraction of active LCCs (i.e., active CaRUs contain active LCCs).

Increased PKA-mediated phosphorylation of LCCs in response to β-AR agonists has also been shown to shift the distribution of LCCs into high-activity gating modes (Chen-Izu et al., 2000; Herzig et al., 1993; Yue et al., 1990). In this study it has been assumed that mode 0_a openings do not significantly contribute to whole-cell I_{CaL} (see Herzig et al.,1993) and are therefore lumped into the inactive population of LCCs. Mode 1 gating of the LCC corresponds to the LCC model control parameter set. Mode 2 gating is defined as a modification of mode 1 parameters based on the data of Yue et al. (1990) in which mean LCC open time is increased from 0.5 ms to 5 ms. This is implemented by reducing the exit rate from the open state (g) (Fig. 1) by a factor of 10. LCC activation and inactivation is shifted by 2 mV in the hyperpolarizing direction in response to ISO consistent with experiments (Chen et al., 2002; Kääb et al., 1996). Under control conditions, all active LCCs are assumed to operate in mode 1, whereas in response to 1 μM ISO, 15% of the active population of LCCs are assumed to operate in mode 2, with 85% remaining in mode 1 (Yue et al., 1990).

β-AR stimulation has also been shown to enhance SERCA2a function (Simmerman and Jones, 1998), reduce inactivation/rectification of I_{Kr} (Heath and Terrar, 2000), and increase amplitude of I_{Ks} (Kathofer et al., 2000). Functional increase in SERCA2a availability is modeled by simultaneous scaling of both the forward and reverse maximum pump rates V_{maxf} and V_{maxr} (Shannon et al., 2000) by a factor of 3.3. Reduction in the degree of steady-state inactivation of I_{Kr} is modeled by reducing rates entering the inactivation state (α_i and α_{i3}) by a factor of 4, and increasing the rates exiting the inactivation state (β_i and Ψ) by this same factor (Mazhari et al., 2001). Functional upregulation of I_{Ks} is modeled by scaling maximal conductance by a factor of 2.

Fig. 2 shows the ability of the baseline model to reproduce experimentally measured β-AR responses to 1 μM ISO. Simultaneous measurements of APs and Ca^{2+} transients are shown in Fig. 2, *A* and *B*, respectively, for control (*black lines*) and after application of ISO (*shaded lines*). APD in response to ISO (Fig. 2 *A*) is shortened by ~30%, plateau potential becomes ~10–15 mV more depolarized, and phase 1 notch depth and duration are reduced. In addition, ISO produces an ~3-fold increase in Ca^{2+} transient amplitude and speeds the relaxation rate of the Ca^{2+} transient ~3-fold (Fig. 2 *B*). The AP generated by the baseline β-AR model (Fig. 2 *C*) exhibits shortening of duration, depolarization of AP plateau, and reduction in phase 1 notch depth and duration similar to that seen experimentally (Fig. 2 *A*). Peak amplitude of the model Ca^{2+} transient (Fig. 2 *D*) is increased ~3-fold and the rate of decay of the transient is increased (shortening its overall duration), as seen in experiments (Fig. 2 *B*).

RESULTS

The shape and duration of the cardiac AP are directly influenced by the dynamical properties of the underlying L-type Ca^{2+} current. Fig. 3 demonstrates that the occurrence and frequency of EAD events are influenced by the modal gating properties of I_{CaL}. A representative train of 20 action potentials, simulated using the full 50,000-CaRU model and paced at 1 Hz with 25% LCCs gating in mode 2, yields a total

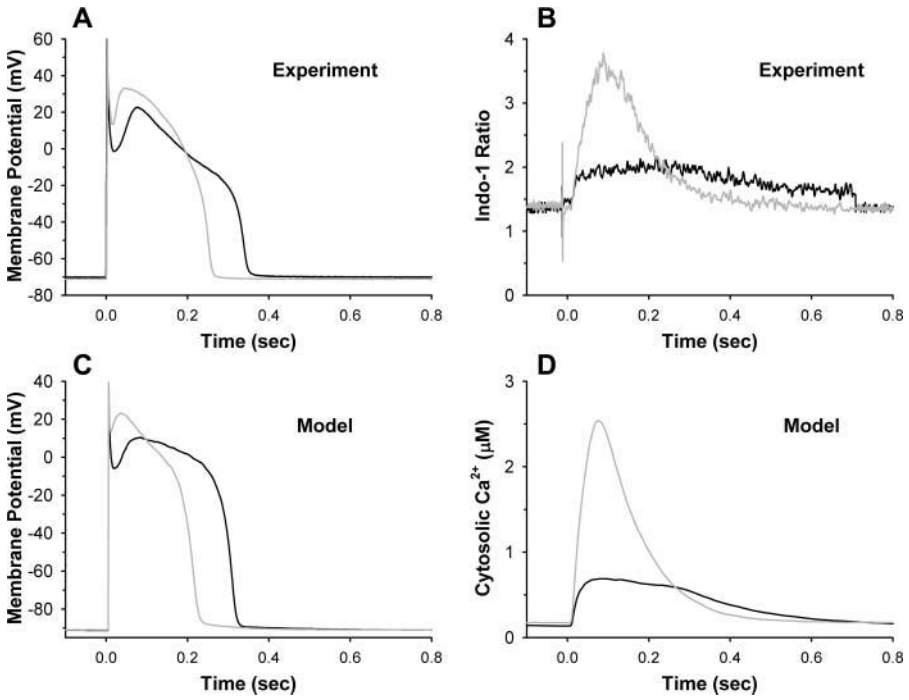

FIGURE 2 Model and experimental APs and Ca^{2+} transients for control (*black*) and β-AR stimulation (*shaded*). (*A*) Representative APs measured in isolated canine myocytes in control bath (*black*) and ISO (*shaded*). (*B*) Indo-1 fluorescence ratio measured simultaneously with the APs in panel *A* (Greenstein et al., 2004). (*C*) Control (*black*) and β-AR stimulated (*shaded*) model APs. (*D*) Model cytosolic Ca^{2+} concentration (μM) corresponding to the APs in panel *C*. Results in panels *C* and *D* were performed with a model including only 2000 simulated CaRUs.

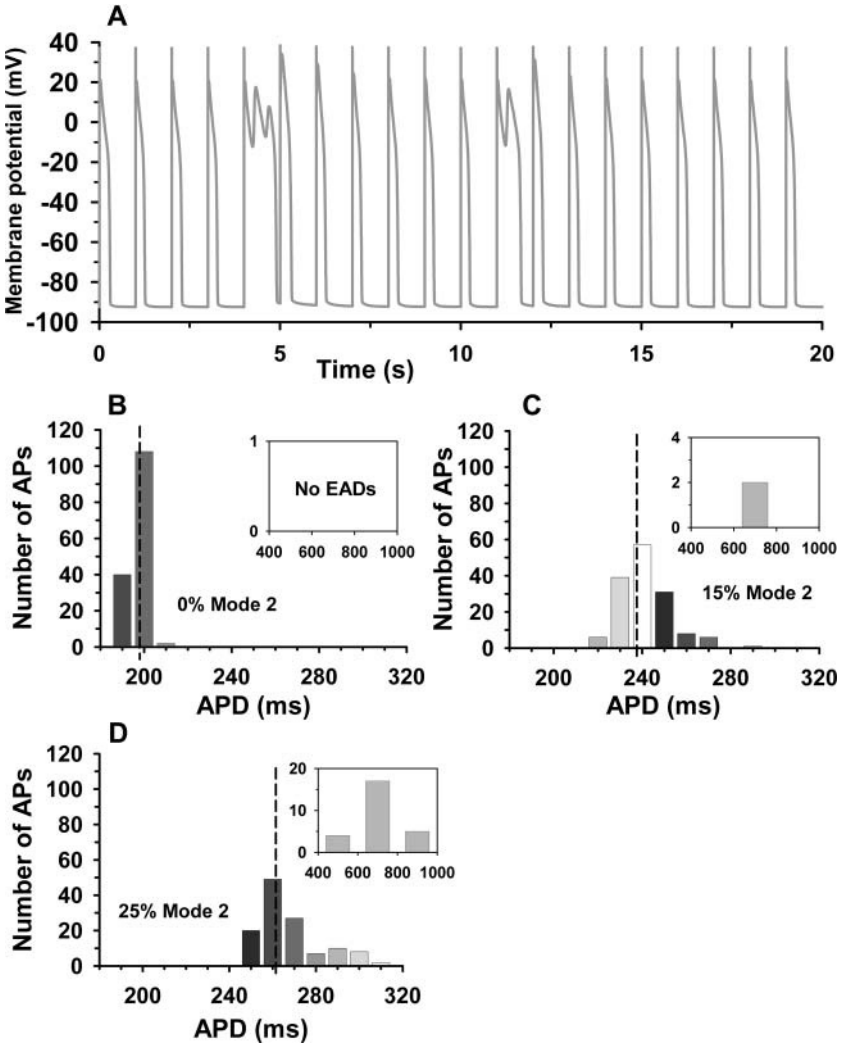

FIGURE 3 (*A*) Membrane potential (*ordinate*, mV) as a function of time (*abscissa*, s) for the baseline β-AR-stimulated model in response to 1 Hz pacing. APD distribution (*ordinate*) in simulations of 150 APs with 0% (*B*), 15% (*C*), or 25% (*D*) of LCCs gating in mode 2 (*abscissa*, 10-ms bins).

of three EADs occurring within two of the APs (Fig. 3 *A*). The timing of EADs appears to be random, i.e., they do not occur at regular time intervals. To better understand the role of modal LCC gating on the frequency dependence of EAD events, long-term simulations were performed. Panels *B*, *C*, and *D* of Fig. 3 show APD distributions measured from a series of 150 APs simulated with 0%, 15%, and 25%, respectively, of LCCs gating in mode 2. In the absence of mode 2 LCCs (Fig. 3 *B*), nearly all APs exhibit a duration in the range of 190–200 ms and no EADs are observed. With 15% of LCCs gating in mode 2 (Fig. 3 *C*), average APD increases to 240 ms, APD variability increases, and two EADs occur (Fig. 3 *C*, *inset*). Further increasing the ratio of mode 2 LCCs to 25% yields an average APD of 263 ms and the rate of EAD occurrence increases dramatically (Fig. 3 *D*, *inset*). These simulation results demonstrate that 1), the rate of EAD occurrence is a monotonic increasing function of the fraction of LCCs gating in mode 2, such that no EADs occur when the fraction is zero; and 2), the average APD increases with increased ratio of LCCs gating in mode 2.

Fig. 4 compares I_{CaL} underlying APs simulated with 0% (*black line*), 15% (*light shaded line*), and 25% (*dark shaded line*) of LCCs operating in mode 2. The shift in composition of I_{CaL} from pure mode 1 to mixed mode 1 and 2 currents has little effect on the peak current magnitude (Fig. 4 *A*). However, the late component of current corresponding to the plateau phase of the AP is enhanced as the ratio of LCCs in mode 2 is increased (Fig. 4 *B*). To clarify this effect, the stochastic gating noise in the L-type current signal has been reduced by averaging I_{CaL} over 10 APs (Fig. 4 *C*), demonstrating that an increased occupancy of mode 2 results in an increased mean I_{CaL} during the plateau. This increase in sustained inward I_{CaL} underlies the observed relationship between APD prolongation and mode 2 occupancy (Fig. 3).

Stochastic nature of EADs

The occurrence of EADs in this model is stochastic in nature due to the gating noise inherent in I_{CaL}. Fig. 5 *A* demonstrates two model APs simulated during β-adrenergic stimulation

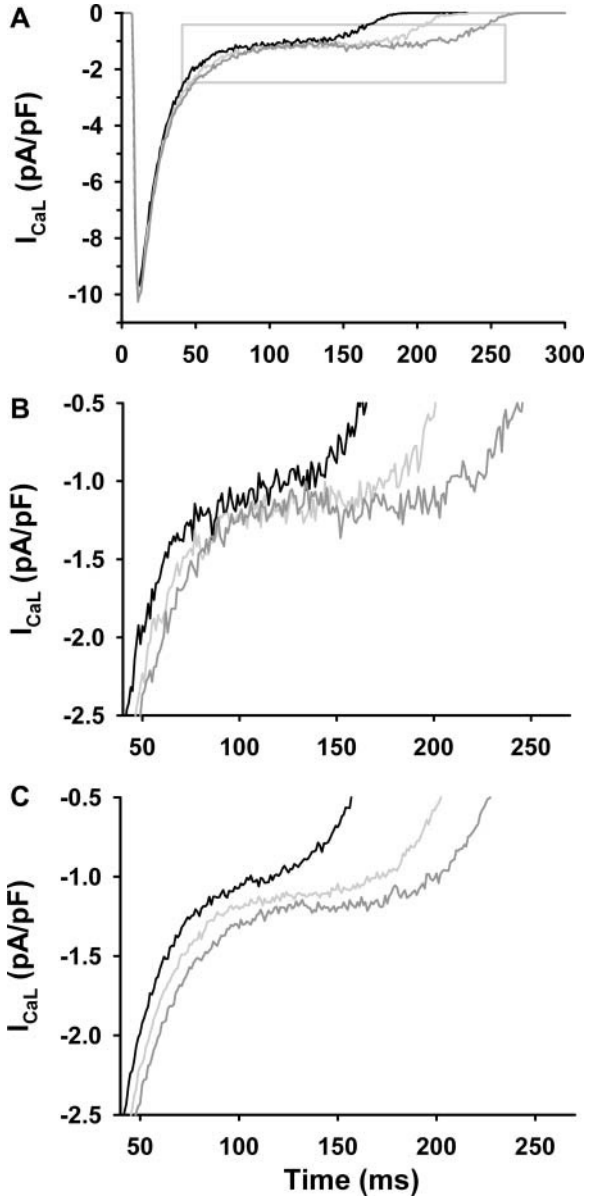

FIGURE 4 Total I_{CaL} (*ordinate*, pA/pF) during a normal AP with 0% (*black*), 15% (*light shaded*), and 25% (*dark shaded*) of LCCs gating in mode 2, plotted against time (*abscissa*, ms). (*A*) Total I_{CaL} during an AP demonstrating little effect of modal fraction on peak current amplitude. (*B*) Blow-up of boxed area in panel *A* during the AP plateau. (*C*) Total I_{CaL} averaged over 10 APs during the AP plateau.

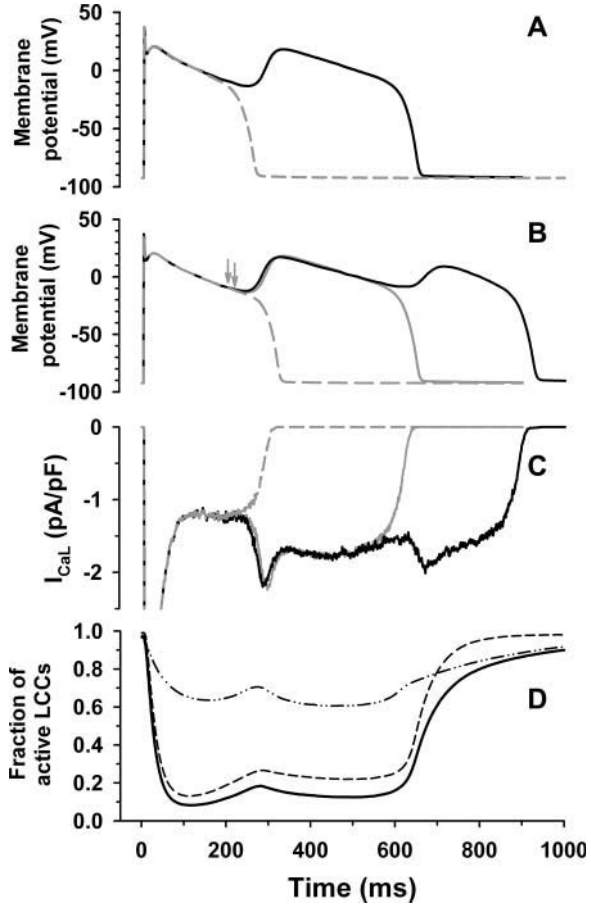

FIGURE 5 (*A*) Membrane potential (*ordinate*, mV) as a function of time (*abscissa*, ms) for two AP simulations in which model parameters, state variable initial conditions, and initial states of each channel are identical, where only the random number generator seeds are initialized to different values. (*B*) Membrane potential (*ordinate*, mV) as a function of time (*abscissa*, ms) for three AP simulations in which the random number generator seeds are reinitialized from the single-EAD AP (*solid shaded line*) to different values at 140 ms (*dashed shaded line*) and 170 ms (*solid black line*) after the stimulus, resulting in a non-EAD AP and a two-EAD AP, respectively. (*C*) L-type Ca^{2+} currents corresponding to the three APs shown in panel B. (*D*) Ratio of LCCs (*ordinate*) that have not inactivated via the voltage-dependent (*dash-dotted line*), the Ca^{2+}-dependent (*dashed line*), or either (*solid line*) mechanism, plotted against time (*abscissa*, ms).

using the full 50,000-CaRU model. Model parameters and initial conditions are identical for both APs shown. However, different seeds are used to initialize the pseudorandom number generator, thus yielding different realizations of LCC and RyR gating during each of the two APs. One of the APs exhibits an EAD, whereas the other does not. This behavior demonstrates that in the presence of LCC mode 2 gating, purely stochastic gating events (i.e., different realizations of the same gating scheme) can determine whether or not an EAD is triggered, in contrast to earlier models in which EADs occur deterministically (Zeng and Rudy, 1995). Stochastic events during the plateau and ''second plateau'' following an EAD can trigger additional EADs. A non-EAD, a single-EAD, and a double-EAD AP are shown in Fig. 5 *B*. Using the single-EAD AP as a test case, the random number generator seed was reset at 150 ms and 180 ms (Fig. 5 *B*, *arrows*), leading to the elimination of the EAD and to the appearance of a second EAD, respectively. These results show that there appears to be a critical time during the late plateau of the AP, where the cell may either repolarize or depolarize (into an EAD), and that the outcome as to which of these events occurs is a random event determined by the stochastic gating of LCCs.

Fig. 5 *C* shows I_{CaL} associated with each of the three APs shown in Fig. 5 *B*. A large rapid increase of I_{CaL} coincides with EAD onset. The time course of I_{CaL} inactivation mechanisms corresponding to the single-EAD AP of Fig. 5 *B* is shown in Fig. 5 *D*. The ratio of LCCs that are not in an inactivated state (*solid black line*) reaches a minimum at ~120 ms (corresponding to maximal LCC inactivation), and then proceeds to gradually increase. Both voltage- and Ca^{2+}-dependent inactivation (*dashed* and *dash-dotted lines*, respectively) of the LCCs have partially recovered at the time of onset of the EAD (~260 ms). The results of Fig. 5 *D* show that 10.2% of the LCC population recover from inactivation by the time of EAD onset. Of these, 9.5% recover from Ca^{2+}-dependent inactivation, whereas only 1.4% recover from *V*-dependent inactivation. The overlap of these population subsets represents 0.7% of LCCs which recover from both Ca^{2+}- and *V*-dependent inactivation. This demonstrates that preceding the EAD, LCC recovery from inactivation is due primarily to recovery from the Ca^{2+}-mediated inactivation state (i.e., transitions from Mode Ca to Mode Normal in the model). This recovery from inactivation is necessary to provide a sufficient number of available LCCs, and hence a sufficient amount of inward current for an EAD to be triggered successfully.

The nature of the current fluctuations in I_{CaL} differ for mode 1 and mode 2 LCC populations. To elucidate how channels in each mode contribute to the mechanism of EAD generation, the model currents are separated in the following analyses. Fig. 6, *A–C*, shows total I_{CaL}, mode 1 I_{CaL}, and mode 2 I_{CaL}, respectively, corresponding to APs both with (*black line*) and without (*shaded line*) an EAD. The timescale is chosen to show the detail at the time of onset of the EAD. These two AP simulations differ only by a change in the random number generator seed at 160 ms. There is little difference between non-EAD and EAD currents preceding 235 ms, at which time the two currents begin to diverge, where the non-EAD current begins to decrease in amplitude, whereas the other grows in amplitude indicating the start of the EAD. A small spike in inward mode 2 current (Fig. 6 *C*, *arrow*) occurs at 232 ms and may be an EAD triggering event. Immediately after this event, an inward current deflection is observed in both mode 1 (Fig. 6 *B*, *arrow*) and total I_{CaL} (Fig. 6 *A*, *arrow*) at 235 ms. This inward deflection in I_{CaL} may be sufficient to trigger an EAD; however, events such as these are generally difficult to identify because the magnitude of inward LCC current deflection preceding an EAD is comparable to the range in which deflections occur at other time points during the plateau of the AP. For this reason, it cannot be determined whether these brief events are in fact playing a role in the trigger mechanism of EADs.

Power spectral analysis can be performed on I_{CaL} to better understand the relationship between mode 2 occupancy fraction and frequency content of the gating noise. Power spectra of I_{CaL} are calculated using Burg's method (Percival and Walden, 1993) for simulations with 0% (*solid black line*), 15% (*dark shaded dashed line*), and 25% (*light shaded dashed line*) of LCCs in mode 2. Currents are recorded during a voltage-clamp simulation, in which the cell is first held at −90 mV for 3 s, stepped to 40 mV for 10 ms, and then stepped to 5 mV for 7 s. Spectral analysis is performed on currents obtained during the final 5 s of this protocol and the results are shown in Fig. 7 *A*. The results indicate that the amplitude of slow-timescale (low-frequency) fluctuations of I_{CaL} does not depend upon frequency and increases as the fraction of LCCs gating in mode 2 increases. There is an ~7-dB/Hz, or fivefold, difference in power between I_{CaL} composed purely of mode 1 channels and that containing 50% mode 2 channels. This corresponds to a 2.2-fold difference in current amplitude in the low-frequency range. At high frequencies, the power drops off as $1/f^a$ where *a* is ~2. These results agree with theoretical calculations, which predict that the power spectral density for a collection of ion channels with exponentially distributed open times is flat at low frequencies (i.e., white noise) and is decreasing at high frequencies with slope

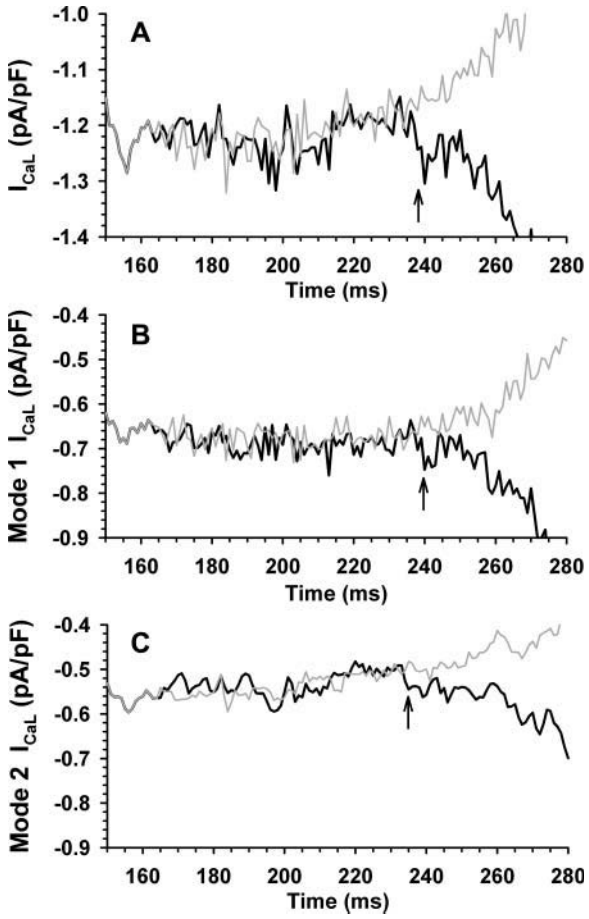

FIGURE 6 (*A*) Total Ca^{2+} current through LCCs (*ordinate*, pA/pF) during an EAD (*black*), compared with currents from a non-EAD AP (*shaded*) plotted against time (*abscissa*, ms). (*B*) Mode 1 and (*C*) mode 2 LCC current components (*ordinate*, pA/pF) of the currents in panel *A*, plotted against time (*abscissa*, ms).

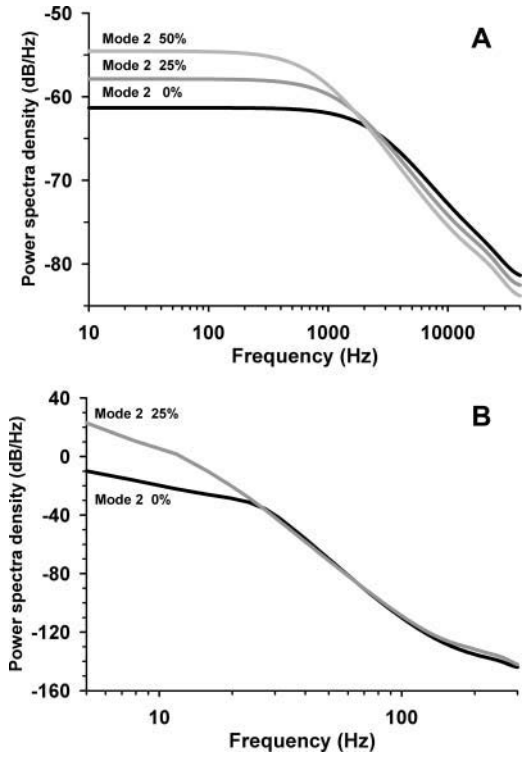

FIGURE 7 (*A*) Power spectra (*ordinate*, dB/Hz) of detrended total I_{CaL} with 0% (*solid black*), 25% (*dark shaded*), and 50% (*light shaded*) of LCCs gating in mode 2, plotted against frequency (*abscissa*, Hz). (*B*) Average power spectra (*ordinate*, dB/Hz) of voltage fluctuations averaged over 10 APs with 0% (*solid black*) and 25% (*dark shaded*) of LCCs gating in mode 2, plotted against frequency (*abscissa*, Hz).

proportional to $1/f^2$. The boundary between these regions is expected to occur at a frequency which corresponds to the timescale of channel gating, and occurs in the range of 0.5–1.5 ms in this model. These results indicate that the presence of mode 2 channels significantly increases the amplitude of I_{CaL} fluctuations at a timescale slower than 1 ms.

The properties of fluctuations in membrane potential during an AP are determined by both the noise in I_{CaL} as well as overall membrane impedance. Fig. 7 *B* shows the power spectrum of voltage noise for APs simulated with 0% (*solid black line*) and 25% (*dark shaded line*) of LCCs gating in mode 2. Only membrane potential during the AP plateau is analyzed. This is accomplished using a window of 250 ms duration starting at the time when membrane potential crosses +15 mV. Each signal is detrended by subtraction of the mean AP profile. Spectra are calculated for the plateau of each AP in a series of 10 beats and averaged. The results indicate that an increase in the fraction of channels gating in mode 2 from 0% to 25% leads to a substantial increase in the amplitude of slow-timescale (low-frequency) fluctuations in voltage. These results indicate that the presence of LCCs gating in mode 2 significantly increases the amplitude of voltage fluctuations at a timescale slower than 40 ms, which results in increased APD variation, and hence leads to an enhanced propensity for EAD formation.

DISCUSSION

Experimental data indicate that LCC phosphorylation events which promote mode 2 gating of LCCs, such as β-AR stimulation and increased expression of CaMKII (Chen-Izu et al., 2000; Dzhura et al., 2000; Yue et al., 1990), contribute to the generation of EADs (De Ferrari et al., 1995; Priori and Corr, 1990; Volders et al., 1997; Wu et al., 2002). We have tested the hypothesis that increased mode 2 gating induces EADs. Modeling results demonstrate that an increase in the ratio of LCCs gating in mode 2 favors the occurrence of EADs via a mechanism whereby the likelihood of such events is raised by stochastic prolongation of APD and subsequent reactivation of LCCs. Results of this study demonstrate that 1), the rate of EAD occurrence in response to long-term (150-s) 1-Hz pacing is a monotonic increasing function of the fraction of LCCs gating in mode 2, where no EADs occur if that fraction is zero (Fig. 2 *A*); 2), when the fraction of LCCs gating in mode 2 is >0, EAD occurrence is a stochastic event; and 3), the random opening of a sufficient number of LCCs gating in mode 2 can initiate an EAD (Figs. 3 and 7).

Mechanism of EAD formation

Generation of an EAD requires an inward current that is sufficiently large that total membrane current becomes inward. The main ionic current candidates that may be responsible for inducing EADs are therefore I_{CaL} and I_{NCX} (Na^+-Ca^{2+} exchanger). I_{NCX} did not play a significant role in EAD generation in this model (data not shown), whereas the role of I_{CaL} is evident from Fig. 5, *B* and *C*, where the increase in magnitude of I_{CaL} coincides with the onset of each EAD.

In the β-AR stimulated model of the canine cardiac myocyte, EADs have been shown to be stochastic events (Fig. 3). Variation in I_{CaL} due to stochastic gating of LCCs leads to variation in APD, and hence some APs are prolonged. These prolonged APs exhibit an increased likelihood of EAD occurrence since the time available for LCC to recover from Ca^{2+}-mediated inactivation is extended during the AP plateau and recovered channels are likely to reopen, possibly triggering an EAD. Even when these conditions are present, however, an EAD is not guaranteed to occur because it is an inherently stochastic event that depends upon the number and duration of LCC openings during the late plateau of the AP. This is demonstrated in Fig. 5 *B*, where changes in the random number generator seeds late in the plateau of a single EAD-AP can either eliminate the EAD or produce an additional EAD within the same AP. This behavior demonstrates that the trajectory of an AP is bistable, as small changes in I_{CaL} (of a magnitude

comparable to the noise in this current) can dramatically alter the morphology of the AP. This behavior is a form of stochastic resonance (see, e.g., White et al., 2000) which relies upon intrinsic noise levels in I_{CaL} and the fact that net membrane current is small during the plateau.

The effect of increasing the ratio of mode 2 LCCs can be separated into two components: 1), an increase in the mean amplitude of the sustained inward Ca^{2+} current during plateau, which prolongs AP in a deterministic manner (Fig. 4); and 2), an increase in slow-timescale fluctuations of total I_{CaL} (Fig. 7 *A*), which enhances the likelihood of EAD triggering due to increased variation in APD (Figs. 3, *B–D*, and 7). Interestingly, the balance between mode 1 and mode 2 LCCs does not significantly influence the peak amplitude of I_{CaL}.

The relationship between noise in I_{CaL} and noise in membrane potential can be deduced from Fig. 7. The addition of mode 2 channels to I_{CaL} enhances the amplitude of current fluctuations at timescales slower than 1 ms, whereas the enhancement of fluctuation in membrane potential is limited to timescales slower than 40 ms. This is a theoretically expected feature of this relationship since membrane impedance is low-pass in nature. In addition, the power spectrum of membrane potential may be influenced by time-dependent changes in membrane impedance during the AP. However, calculation of instantaneous *I-V* curves during the AP plateau time interval that was used to calculate power spectra indicates that membrane conductance does not change significantly over this interval (data not shown). The spectral properties of voltage noise are therefore largely determined by fluctuations of I_{CaL} during the AP plateau, rather than fluctuation of membrane impedance.

Injection of an external current during the late plateau of an AP during β-adrenergic stimulation can induce an EAD. The strength-duration relationship for an EAD-inducing square current pulse is quasihyperbolic, such that the current amplitude required to induce an EAD is quite small for a long duration pulse (data not shown). This system property suggests that modest amplification of slow-timescale fluctuations could effectively increase the likelihood of triggering EADs, and this is precisely what occurs as a fraction of the LCCs transition to mode 2 activity (Fig. 7). This result demonstrates that the appearance of LCCs with a long mean open time can have a profound impact on AP profile, even if only a small fraction of channels exhibit these high-activity gating dynamics.

To reduce computational load, not all simulations were run with the full 50,000-CaRU model. Reduction of the number of simulated CaRUs increases the variance of I_{CaL}, which may in turn produce an increased frequency of EADs in the simulations presented in Fig. 3, *B–D* (compared to the full model). This increase in I_{CaL} noise, however, does not influence the interpretation of the results regarding the mechanism of EAD generation. Both the full 50,000-CaRU model (Fig. 3 *A*) and the reduced 10,000-CaRU model (Fig. 3, *B–D*) exhibit EADs only in the presence of LCCs gating in mode 2. In the absence of mode 2 gating of LCCs both the full and the reduced models fail to exhibit EADs in runs as long as 400 s at 1 Hz (data not shown). Regardless of the number of CaRUs simulated, the mechanism of EAD generation was consistently observed to be dependent on stochastic gating of LCCs (Fig. 5, *A* and *B*).

Comparison with previous studies

In traditional approaches to myocyte modeling, it has often been assumed that it is sufficient to simulate the behavior of a large number (10^5–10^7) of ion channels using equations that describe the expected (average) behavior of the channel population. In this approach, fluctuations about the average behavior are assumed to be insignificant with respect to whole-cell dynamics.

Previous studies in the neuron (Chow and White, 1996; White et al., 1998, 2000) have shown that in the presence of a small number of stochastically gating ion channels, spontaneous action potentials can be triggered in a random pattern. For a population of independent identical channels, the central limit theorem states that as the number of channels (N) increases, the standard deviation in the signal will scale as $N^{-1/2}$ (Feller, 1970), indicating that the amplitude of the gating noise may not be so small as to be considered inconsequential. This property coupled with the nonlinear bistability exhibited by the myocyte late in the AP plateau, results in a system where gating noise can contribute to the triggering of EADs in the presence of a physiological number of channels (40,000–200,000 LCCs).

Experimental measurements have demonstrated that gating noise may be the primary source of APD variability (Zaniboni et al., 2000). The coefficient of variation of APD in guinea pig ventricular myocytes (without β-AR stimulation) has been measured to be $2.3 \pm 0.9\%$, and $1.3 \pm 0.4\%$ in the absence of the late Na^+ current (Zaniboni et al., 2000). In the baseline canine myocyte model (which does not include a late Na^+ current), in the absence of β-AR stimulation, coefficient of variation of APD is 1.4% with all 12,500 CaRUs included in the simulation, which agrees well with the experimental value.

Electrotonic coupling effects have been shown to have a major influence on the generation and propagation of EADs in myocardial tissue. A recent study by Zaniboni et al. (2000) demonstrated that EADs in single isolated myocytes were suppressed when the EAD-producing myocyte was electrically coupled to a normal myocyte. It is likely that in the presence of electrotonic loading, there must be a critical mass of cells that generate near simultaneous EADs for propagation to occur. This is an important consideration with respect to any mechanism of generation of EADs at the cellular level, including the mechanism considered here. However, it is important to understand all possible mechanisms by which EADs may be generated at the cellular level. It is known that

EAD frequency is increased in ventricular myocytes isolated from the failing heart (Nuss et al., 1999), likely due to hyperphosphorylation of LCCs (Chen et al., 2002). Overexpression of CaMKII in isolated murine myocytes, which increases mode 2 gating of LCCs, leads to increased EAD frequency (Wu et al., 2002). Our results provide a possible explanation for these experimental data. Overexpression of CaMKII is also shown to produce EADs in murine ventricular tissue and these EADs are eliminated with application of CaMKII inhibitors, with little or no accompanying APD shortening (Wu et al., 2002). These data demonstrate that under these particular experimental conditions, EADs produced by increased mode 2 gating of LCCs may occur in tissue. The precise mechanism(s) by which EAD generation is supported at the tissue level remains an important issue that is central to the interpretation of our results. We are currently working on methods to further optimize simulation runtime, and plan to address this issue once more efficient algorithms have been developed.

In the LCC model used in this study, mode 2 activity differs from that of mode 1 only in channel mean open time. Recently, Josephson et al. (2002a,b) have found that mode 2 LCCs exhibit a 70% increase in unitary current amplitude compared to mode 1 channels, as well as a shift in the voltage dependence of channel opening. Mean open time was also observed to be 10–100 times greater for mode 2 channels than for mode 1 channels. Inclusion of these experimental findings would likely enhance the contribution of mode 2 LCC fluctuations to total I_{CaL}, further supporting the idea that modal gating of LCCs is an important component of the mechanism of EAD generation.

Calmodulin kinase II and EADs

The effects of CaMKII on cardiac myocytes are under intensive investigation (reviewed in Anderson, 2004). Recent evidence obtained in the presence of constitutively active CaMKII indicate that 1), there is a significant shift in LCC gating from mode 1 to mode 2 (Dzhura et al., 2000); and 2), myocytes isolated from transgenic mice exhibit both EADs and enhanced LCC activity (open probability) (Wu et al., 2002). Both of these effects are eliminated by the CaMKII-inhibiting peptide AC3-I. The agreement of our simulation results with these experiments suggests that phosphorylation targets of CaMKII are likely similar to those of PKA as implemented in this study. Wu et al. (2002) also observed that the decrease in EAD frequency with CaMKII inhibition was not associated with a decrease in APD, suggesting that AP prolongation alone does not cause EADs. The modeling results presented here suggest that an altered distribution of LCCs among modes, combined with altered channel availability, can influence the frequency of EADs in the absence of a change in APD, and therefore may be an important mechanism underlying these experimental observations.

CONCLUSIONS

The results presented here suggest that the traditional approach to building models of excitable cells by implementing descriptions of the expected (average) behavior for each population of ion channels may in some instances fail to capture important cellular phenomena. Fluctuations in cell signals about their average value can induce dramatic qualitative changes in cell behavior as a result of stochastic resonance. In the cardiac myocyte model used here, the rate of EAD occurrence was shown to be enhanced by mode 2 L-type channel gating via a mechanism that depends upon an increase in both the average current level and the amplitude of low-frequency fluctuations in the current.

Recent evidence indicates that in human heart failure, the number of LCCs expressed is reduced and the fraction of LCCs available for gating is increased (Schröder et al., 1998). It has been suggested that the phosphorylation of protein targets within the cellular microdomain between the *t*-tubule and the JSR may be regulated locally, and that the phosphorylation state of these molecules is increased in failing human ventricular myocytes, potentially as a result of decreased activity of phosphatases in the microdomain (Chen et al., 2002). We therefore speculate that the stochastic mechanism of EAD generation investigated in this simulation study may also be of importance in explaining the increased rate of EAD occurrence in failing ventricular myocytes (Nuss et al., 1999). There is as yet no evidence of any shift in the relative distribution of LCC gating modes in human heart failure. Experimental studies directed at understanding details of LCC modal gating in both normal and diseased human myocytes would be an important direction for future investigation.

The model presented here can be found on the Center for Cardiovascular Bioinformatics and Modeling web site (http://www.ccbm.jhu.edu/).

This work was supported by National Institutes of Health grants RO1 HL60133, RO1 HL61711, and P50 HL52307, the Falk Medical Trust, the Whitaker Foundation, and IBM.

REFERENCES

Anderson, M. E. 2004. Calmodulin kinase and L-type calcium channels: a recipe for arrythmias? *Trends Cardiovasc. Med.* 14:152–161.

Chen, X., V. Piacentino III, S. Furukawa, B. Goldman, K. B. Margulies, and S. R. Houser. 2002. L-type Ca2+ channel density and regulation are altered in failing human ventricular myocytes and recover after support with mechanical assist devices. *Circ. Res.* 91:517–524.

Chen-Izu, Y., R. P. Xiao, L. T. Izu, H. Cheng, M. Kuschel, H. Spurgeon, and E. G. Lakatta. 2000. G(i)-dependent localization of beta(2)-adrenergic receptor signaling to L-type Ca(2+) channels. *Biophys. J.* 79:2547–2556.

Chow, C. W., and J. A. White. 1996. Spontaneous action potentials due to channel fluctuations. *Biophys. J.* 71:3013–3021.

De Ferrari, G. M., M. C. Viola, E. D'Amato, R. Antolini, and S. Forti. 1995. Distinct patterns of calcium transients during early and delayed afterdepolarizations induced by isoproterenol in ventricular myocytes. *Circulation.* 91:2510–2515.

De Jongh, K. S., B. J. Murphy, A. A. Colvin, J. W. Hell, M. Takahashi, and W. A. Catterall. 1996. Specific phosphorylation of a site in the full length form of the α1 subunit of the cardiac L-type calcium channel by adenosine 3′,5′-cyclic monophosphate-dependent protein kinase. *Biochemistry.* 35:10392–10402.

Dzhura, I., Y. Wu, R. J. Colbran, J. R. Balser, and M. E. Anderson. 2000. Calmodulin kinase determines calcium-dependent facilitation of L-type calcium channels. *Nat. Cell Biol.* 2:173–177.

Engeln-Müllges, G., and F. Uhlig. 1996. Numerical Algorithms with C. Springer-Verlag, Berlin.

Erxleben, C., C. Gomez-Alegria, T. Darden, Y. Mori, L. Birnbaumer, and D. L. Armstrong. 2003. Modulation of cardiac Ca(V)1.2 channels by dihydropyridine and phosphatase inhibitor requires Ser-1142 in the domain III pore loop. *Proc. Natl. Acad. Sci. USA.* 100:2929–2934.

Feller, W. 1970. An Introduction to Probability Theory and Its Applications. Wiley, New York.

Gao, T., A. Yatani, M. L. Dell'Acqua, H. Sako, S. A. Green, A. Drascal, S. D. Scott, and M. M. Hosey. 1997. cAMP-dependent regulation of cardiac L-type Ca^{2+} channels requires membrane targeting of PKA and phosphorylation of channel subunits. *Neuron.* 19:185–196.

Greenstein, J., S. Po, R. Wu, G. Tomaselli, and R. L. Winslow. 2000. Role of the calcium-independent transient outward current Ito1 in action potential morphology and duration. *Circ. Res.* 87:1026–1033.

Greenstein, J., A. J. Tanskanen, and R. L. Winslow. 2004. Modeling the actions of β-adrenergic signaling on excitation-contraction coupling processes. *Ann. N. Y. Acad. Sci.* 1015:16–27.

Greenstein, J. L., and R. L. Winslow. 2002. An integrative model of the cardiac ventricular myocyte incorporating local control of Ca^{2+} release. *Biophys. J.* 83:2918–2945.

Handrock, R., F. Schröder, S. Hirt, A. Haverich, C. Mittmann, and S. Herzig. 1998. Single-channel properties of L-type calcium channels from failing human ventricle. *Cardiovasc. Res.* 37:445–455.

Heath, B., and D. Terrar. 2000. Protein kinase C enhances the rapidly activating delayed rectifier potassium current, IKr, through a reduction in C-type inactivation in guinea-pig ventricular myocytes. *J. Physiol.* 522: 391–402.

Herzig, S., P. Patil, J. Neumann, C.-M. Staschen, and D. Yue. 1993. Mechanisms of β-adrenergic stimulation of cardiac Ca^{2+} channels revealed by discrete-time Markov analysis of slow gating. *Biophys. J.* 65:1599–1612.

Hess, P., J. B. Lansman, and R. W. Tsien. 1984. Different modes of Ca channel gating behaviour favoured by dihydropyridine Ca agonists and antagonists. *Nature.* 311:538–544.

Hobai, I. A., and B. O'Rourke. 2001. Decreased sarcoplasmic reticulum calcium content is responsible for defective excitation-contraction coupling in canine heart failure. *Circulation.* 103:1577–1584.

Imredy, J. P., and D. T. Yue. 1994. Mechanism of Ca^{2+}-sensitive inactivation of L-type Ca^{2+} channels. *Neuron.* 12:1301–1318.

Jafri, S., J. J. Rice, and R. L. Winslow. 1998. Cardiac Ca^{2+} dynamics: the roles of ryanodine receptor adaptation and sarcoplasmic reticulum load. *Biophys. J.* 74:1149–1168.

January, C. T., and J. M. Riddle. 1989. Early afterdepolarizations: mechanism of induction and block—a role for L-type Ca^{2+} current. *Circ. Res.* 64:977–990.

January, C. T., J. M. Riddle, and J. J. Salata. 1988. A model for early afterdepolarizations: induction with the Ca^{2+} channel agonist Bay K 8644. *Circ. Res.* 62:563–571.

Josephson, I. R., A. Guia, E. G. Lakatta, and M. D. Stern. 2002a. Modulation of the conductance of unitary cardiac L-type Ca^{2+} channels by conditioning voltage and divalent ions. *Biophys. J.* 83:2587–2594.

Josephson, I. R., A. Guia, E. G. Lakatta, and M. D. Stern. 2002b. Modulation of the gating of unitary cardiac L-type Ca^{2+} channels by conditioning voltage and divalent ions. *Biophys. J.* 83:2575–2586.

Kääb, S., H. B. Nuss, N. Chiamvimonvat, B. O'Rourke, P. H. Pak, D. A. Kass, E. Marban, and G. F. Tomaselli. 1996. Ionic mechanism of action potential prolongation in ventricular myocytes from dogs with pacing-induced heart failure. *Circ. Res.* 78:262–273.

Kathofer, S., W. Zhang, C. Karle, D. Thomas, W. Schoels, and J. Kiehn. 2000. Functional coupling of human beta 3-adrenoreceptors to the KvLQT1/MinK potassium channel. *J. Biol. Chem.* 275:26743–26747.

Keizer, J., G. D. Smith, S. Ponce-Dawson, and J. E. Pearson. 1998. Saltatory propagation of Ca2+ waves by Ca2+ sparks. *Biophys. J.* 75: 595–600.

Marbán, E., S. W. Robinson, and W. G. Wier. 1986. Mechanisms of arrhythmogenic delayed and early afterdepolarizations in ferret ventricular muscle. *J. Clin. Invest.* 78:1185–1192.

Matsumoto, M., and T. Nishimura. 1998. Mersenne Twister: A 623-dimensionally equidistributed uniform pseudo-random number generator. *ACM Trans. Model. Comput. Sim.* 8:3–30.

Mazhari, R., J. L. Greenstein, R. L. Winslow, E. Marbán, and H. B. Nuss. 2001. Molecular interactions between two long-QT syndrome gene products, HERG and KCNE2, rationalized by in vitro and in silico analysis. *Circ. Res.* 89:33–38.

Mazur, A., D. M. Roden, and M. E. Anderson. 1999. Systemic administration of calmodulin antagonist W-7 or protein kinase A inhibitor H-8 prevents torsade de pointes in rabbits. *Circulation.* 100: 2437–2442.

McDonald, T. F., A. Cavalie, W. Trautwein, and D. Pelzer. 1986. Voltage-dependent properties of macroscopic and elementary calcium channel currents in guinea pig ventricular myocytes. *Pflugers Arch.* 406:437–448.

Nuss, H. B., S. Kääb, D. A. Kass, G. F. Tomaselli, and E. Marbán. 1999. Cellular basis of ventricular arrhythmias and abnormal automaticity in heart failure. *Am. J. Physiol.* 277:H80–H91.

Percival, D. B., and A. T. Walden. 1993. Spectral Analysis for Physical Applications: Multitaper and Conventional Univariate Techniques. Cambridge University Press, Cambridge, UK.

Priori, S. G., and P. B. Corr. 1990. Mechanisms underlying early and delayed afterdepolarizations induced by catecholamines. *Am. J. Physiol.* 258:H1796–H1805.

Rice, J. J., M. S. Jafri, and R. L. Winslow. 1999. Modeling gain and gradedness of Ca(2+) release in the functional unit of the cardiac diadic space. *Biophys. J.* 77:1871–1884.

Roden, D. M. 1993. Early after-depolarizations and torsade de pointes: implications for the control of cardiac arrhythmias by prolonging repolarization. *Eur. Heart J.* 14 (Suppl. H) :56–61.

Rose, W. C., C. W. Balke, W. G. Wier, and E. Marbán. 1992. Macroscopic and unitary properties of physiological ion flux through L-type Ca2+ channels in guinea-pig heart cells. *J. Physiol. (Lond.).* 456:267–284.

Schröder, F., R. Handrock, D. J. Beuckelmann, S. Hirt, R. Hullin, and L. Priebe. 1998. Increased availability and open probability of single L-type calcium channels from failing compared with nonfailing human ventricle. *Circulation.* 98:969–976.

Shannon, T. R., K. S. Ginsburg, and D. M. Bers. 2000. Reverse mode of the sarcoplasmic reticulum calcium pump and load-dependent cytosolic calcium decline in voltage-clamped cardiac ventricular myocytes. *Biophys. J.* 78:322–333.

Simmerman, H. K., and L. R. Jones. 1998. Phospholamban: protein structure, mechanism of action, and role in cardiac function. *Physiol. Rev.* 78:921–947.

Tsien, R., B. Bean, P. Hess, J. Lansman, B. Nilius, and M. Nowycky. 1986. Mechanism of calcium channel modulation by β-adrenergic agents and dihydropyridine calcium agonists. *J. Mol. Cell. Cardiol.* 18:691–710.

Volders, P. G., A. Kulcsar, M. A. Vos, K. R. Sipido, H. J. Wellens, R. Lazzara, and B. Szabo. 1997. Similarities between early and delayed afterdepolarizations induced by isoproterenol in canine ventricular myocytes. *Cardiovasc. Res.* 34:348–359.

White, J. A., R. Klink, A. Alonso, and A. Kay. 1998. Noise from voltage-gated ion channels may influence nauronal dynamics in the entorhinal cortex. *J. Neurophysiol.* 80:262–269.

White, J. A., J. T. Rubinstein, and A. R. Kay. 2000. Channel noise in neurons. *Trends Neurosci.* 23:131–137.

Winslow, R. L., J. J. Rice, M. S. Jafri, E. Marbán, and B. O'Rourke. 1999. Mechanisms of altered excitation-contraction coupling in canine tachycardia-induced heart failure. II. Model studies. *Circ. Res.* 84:571–586.

Wu, Y., J. Temple, R. Zhang, I. Dzhura, W. Zhang, R. Trimble, D. M. Roden, R. Passier, E. N. Olson, R. J. Colbran, and M. E. Anderson. 2002. Calmodulin kinase II and arrhythmias in a mouse model of cardiac hypertrophy. *Circulation.* 106:1288–1293.

Yoshida, A., M. Takahashi, S. Nishimura, H. Takeshima, and S. Kokubun. 1992. Cyclic AMP-dependent phosphorylation and regulation of the cardiac dihydropyridine-sensitive Ca channel. *FEBS Lett.* 309: 343–349.

Yue, D., S. Herzig, and E. Marban. 1990. β-adrenergic stimulation of calcium chanels occurs by potentiation of high-activity gating modes. *Proc. Natl. Acad. Sci. USA.* 87:753–757.

Zaniboni, M., A. E. Pollard, L. Yang, and K. W. Spitzer. 2000. Beat-to-beat repolarization variability in ventricular myocytes and its suppression by electrical coupling. *Am. J. Physiol. Heart Circ. Physiol.* 278:H677–H687.

Zeng, J., and Y. Rudy. 1995. Early afterdepolarizations in cardiac myocytes: mechanism and rate dependence. *Biophys. J.* 68:949–964.

Zhou, J. T., L. R. Zheng, and W. Y. Liu. 1992. Role of early afterdepolarization in familial long QTU syndrome and torsade de pointes. *Pacing Clin. Electrophysiol.* 15:2164–2168.